Graphene Quantum Hall Effect Devices for AC and DC Electrical Metrology

Mattias Kruskopf, Stephan Bauer, Yaowaret Pimsut, Atasi Chatterjee, Dinesh K. Patel, Albert F. Rigosi, Randolph E. Elmquist, *Senior Member, IEEE*, Klaus Pierz, Eckart Pesel, Martin Götz, and Jürgen Schurr

***Abstract*— A new type of graphene-based quantum Hall standards is tested for electrical quantum metrology applications at alternating current (ac) and direct current (dc). The devices are functionalized with $Cr(CO)_3$ to control the charge carrier density and have branched Hall contacts based on NbTiN superconducting material. The work is an in-depth study about the characteristic capacitances and related losses in the ac regime of the devices and about their performance during precision resistance measurements at dc and ac.**

***Index Terms*— Alternating current, dissipation factor, double-shield, epitaxial graphene, magnetocapacitance, magnetotransport, precision measurements, quantized Hall resistance (QHR) standards, quantum Hall effect (QHE), superconducting contacts.**

I. Introduction

WITH the revision of the International System of Units (SI), quantum effects play a key role in the representation of the units [1], [2]. Following these historical changes, National Metrology Institutes (NMIs) are presently developing a universal electrical quantum standard for the realization of the units ohm, farad, and henry based on the quantum Hall effect (QHE) using graphene devices [3]–[10]. GaAs-based quantized Hall resistance (QHR) standards have been used for metrology at direct current (dc) to realize the resistance unit ohm since 1990. Though a few NMIs apply QHR standards at alternating current (ac) for capacitance and impedance calibrations on a regular basis [4], the worldwide adaption of QHE measurement techniques for ac is still progressing at a slower pace due to stringent device property requirements and measurement equipment. The rapid progress in graphene-based QHE device development in metrology has been linked with alleviated measurement requirements when using modern cryogenic systems, which are significantly more user-friendly when compared with the systems using GaAs-based standards [11]. Using the advantages of lower magnetic flux density and higher measurement temperature, graphene-based QHR systems are becoming more compact and easy to use [12], [13]. These changes are accelerating the worldwide adoption of electrical quantum standards in metrology and potentially in industry.

In this work, we report on a joint effort of the Physikalisch-Technische Bundesanstalt (PTB) and the National Institute of Standards and Technology (NIST) to fabricate and test epitaxial-graphene-based QHE devices for electrical quantum metrology in the dc and ac regime. The purpose of the new design using fewer Hall contacts and superconducting materials is to optimize and identify the sample characteristics that are critical to the measurement precision, especially in the ac regime [14].

II. Device Characteristics and Transport Properties

A batch of several graphene Hall devices on SiC substrate were fabricated in the facilities of the NIST in Gaithersburg [15]–[17], of which two were characterized at the PTB in Braunschweig. The devices apply a reworked contact design with source/drain and Hall contacts that are split into several branches. This design integrates the principle of the Delahaye multiple-series connection into a single contact, which minimizes the contact resistances in the quantum Hall regime [17], [18]. The labels and configuration of the electrical contacts can be understood from Fig. 4(a). All the measured Hall bars have a total length of 800 μm, a width of 200 μm, and a distance between two neighboring Hall contacts of 200 μm. Additionally, the contacts feature a layer of superconducting NbTiN to further minimize the contact resistance, and the number of Hall contacts is reduced to eliminate a source of capacitive losses [19], [20] when measuring

Manuscript received February 17, 2021; revised April 26, 2021; accepted May 15, 2021. This work was partially supported by the Joint Research Project GIQS (18SIB07). This project received funding from the European Metrology Programme for Innovation and Research (EMPIR) co-financed by the Participating States and from the European Unions' Horizon 2020 research and innovation program. The review of this article was arranged by Editor F. Schwierz. *(Corresponding author: Mattias Kruskopf.)*

Mattias Kruskopf, Stephan Bauer, Atasi Chatterjee, Klaus Pierz, Eckart Pesel, Martin Götz, and Jürgen Schurr are with the Physikalisch-Technische Bundesanstalt, 38116 Braunschweig, Germany (e-mail: mattias.kruskopf@ptb.de).

Yaowaret Pimsut is with the Physikalisch-Technische Bundesanstalt, 38116 Braunschweig, Germany, and also with the National Metrology Institute, Pathum Thani 12120, Thailand.

Dinesh K. Patel is with the Graduate Institute of Applied Physics, National Taiwan University, Taipei 10617, Taiwan.

Albert F. Rigosi and Randolph E. Elmquist are with the National Institute of Standards and Technology, Gaithersburg, MD 20899 USA.

Color versions of one or more figures in this article are available at https://doi.org/10.1109/TED.2021.3082809.

Digital Object Identifier 10.1109/TED.2021.3082809

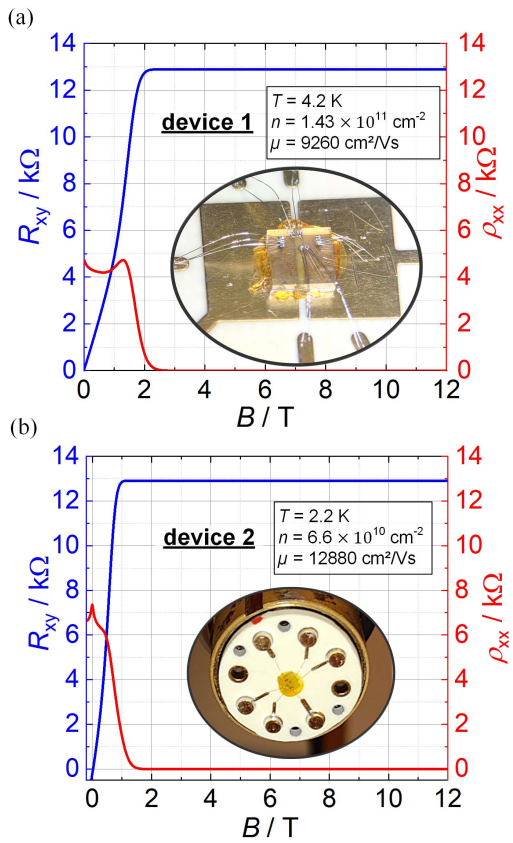

Fig. 1. Characterization of the dc properties of device 1 and device 2. (a) Magnetotransport measurements of device 1. The inset shows the Hall bar glued on a chip carrier with a bottom split shield used for magnetocapacitance measurements. The top shield was removed for the photograph. (b) Measurements of device 2 with lower carrier density. The inset shows a photograph of the mounted device in a euromet chip carrier, which did not apply any shields.

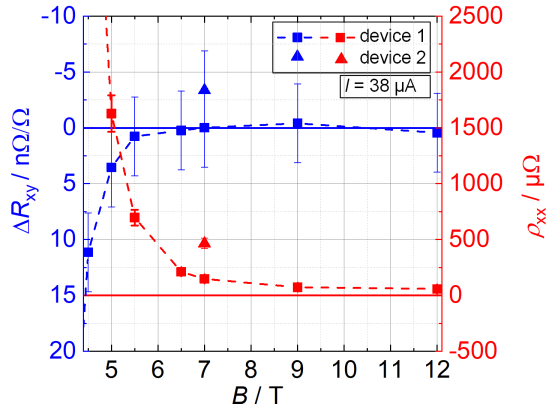

Fig. 2. Precision characterization of device 1 and device 2 at dc. A CCC was used to determine the deviation from the expected resistance value ($R_K/2$) and the longitudinal resistivity ρ_{xx} at the low potential side. The measurements of device 1 revealed a resistivity at the low-potential side of $\rho_{xx} \leq 73\ \mu\Omega \pm 12.5\ \mu\Omega$ for 9 T $\leq B \leq$ 12 T. For device 2, $\rho_{xx} = 466\ \mu\Omega \pm 47\ \mu\Omega$ at $B = 7$ T was found. Device 1 was well-quantized at magnetic flux densities between 5.5 T $\leq B \leq$ 12 T on the order of 1 nΩ/Ω ± 3.5 nΩ/Ω. In the case of device 2, a deviation from nominal of −3.4 nΩ/Ω ± 3.5 nΩ/Ω was found at $B = 7$ T. The stated uncertainties describe the combined uncertainties ($k = 1$).

at ac. In previous works on similar devices with branched NbTiN/Au/Pd/graphene contacts, contact resistances on the order of 100 $\mu\Omega$ were found [17]. The charge carrier density of the graphene devices was in all cases adjusted to a n-type carrier density in the lower range of $n \approx 1 \times 10^{11}$ cm^{-2} by functionalization with $Cr(CO)_3$ and subsequent annealing at 150 °C in an inert gas atmosphere as described in the literature [21]. Both the devices were characterized in a ^{4}He bath cryostat at magnetic flux densities up to $B = 12$ T. Fig. 1(a) and (b) shows the dc magnetotransport properties with a charge carrier density of $n = 1.43 \times 10^{11}$ cm^{-2} and a mobility of $\mu = 9260$ cm^2/Vs for device 1 as well as $n = 6.6 \times 10^{10}$ cm^{-2} and $\mu = 12880$ cm^2/Vs for device 2. Since graphene quantum Hall devices with charge carrier density below $n = 1 \times 10^{11}$ cm^{-2} are often not well-quantized due to charge puddles [22], the temperature of device 2 was lowered to 2.2 K. In the case of device 1, a higher temperature of 4.2 K was adequate. The devices were mounted in a TO-8 (device 1) and Euromet (device 2) [23] chip carriers, with modifications specifically designed for ac measurements. The TO-8 chip carrier of device 1 applied a double shield that is composed of electrodes above and below the device which are split into two parts in the center. The device is mounted such that the pair of Hall contacts are aligned with the gap of the double shield [24]. The double-shield principle was originally designed to allow for tuning the capacitive losses by applying voltages to the electrode of the left side of the shield and shorting the right side of the shield to the low potential current terminal [8], [25]. However, the floating side of the shield [active electrode in Fig. 4(a)] can also be used as an electrode to measure the capacitive components when no external voltages are applied [26], [27] which is the case in this study. The horizontal distance between the left and right sides of the shield is 400 μm, while the vertical distance between the graphene and both the top and bottom electrodes is about 500 μm. Further details about the setup are given in Section IV and Fig. 4(a). Device 2 did not apply shields or gates, but has a nonmetallic base.

III. DC Precision Measurements

While the Hall plateaus in Fig. 1(a) and (b) indicate an onset of resistance quantization at magnetic flux densities between $B = 1.5$ T and $B = 3$ T, precision measurements with a cryogenic current comparator (CCC) resistance bridge are necessary to identify the point of accurate quantization which is usually reached at significantly higher fields. Fig. 2 shows the longitudinal resistivity ρ_{xx} and the deviation from nominal $\Delta R_{xy} = (R_H - R_K/2))/(R_K/2)$ of the two devices, where R_H is the measured Hall resistance, and $R_K \approx 25812.8\ \Omega$ is the von Klitzing constant. Both the quantities, ρ_{xx} and ΔR_{xy}, were determined with a CCC using a stable 100 Ω reference resistor. The plotted uncertainties describe the combined type A and type B uncertainties ($k = 1$), taking into account the drift and calibration procedure of the reference resistors as well as the geometrical factors of the devices. For magnetic flux densities of $B \geq 5.5$ T, the Hall resistance of device 1 agrees with the quantized

value $R_K/2$ to within a few nΩ/Ω. However, the rather high ρ_{xx} values indicate a relatively broad transition region of several tesla at the edge of the resistance plateau. Typical ρ_{xx} values of well-quantized graphene QHE devices below 100 $\mu\Omega$ were found for flux densities $B \geq 9$ T. Device 2 did not show ideal prerequisites for dc QHR standards [28], [29] due to the relatively high resistivity of $\rho_{xx} = 465.5\ \mu\Omega \pm 47\ \mu\Omega$ at the applied magnetic flux density of $B = 7$ T. However, the Hall resistance still agreed with $R_K/2$ within the type B uncertainty of the reference resistor, which shows that only a small portion of the longitudinal resistance was mixing into the Hall resistance. The calculated S-parameters of both the devices at all applied B-field values were below ±0.1.

IV. AC Characterization

The first characterization steps of a QHR device in the dc and ac domains are very similar and are the same for graphene or GaAs-based devices. Initially, the ac contact resistances were determined with a simple three-terminal-pair measurement with the device in the quantized state. The contact resistances were found to be zero within the measurement uncertainty of 10 mΩ at 1000 Hz. The contact resistance is not expected to be significantly frequency-dependent. The longitudinal resistance at the low potential side of the Hall bar at ac was measured with a relatively simple setup that applies a lock-in amplifier as the source and detector (SR 850 DSP lock-in amplifier, Stanford Research Systems†) using the setup as described in [30]. In general, the ac longitudinal resistance is equal to the dc longitudinal resistance plus the dissipation caused by capacitive coupling in the 2-D electron gas. The setup was adjusted at a point of good quantization that initially was determined with the CCC and was then kept unchanged while continuously sweeping the magnetic flux densities and measuring the real part of the longitudinal resistance ρ_{xx} within the Hall resistance plateau. For measurements of the frequency dependence at fixed B-field values, the setup is readjusted at each frequency.

The ac measurement results of ρ_{xx} of device 1 between $B = 5$ T and $B = 12$ T at frequencies up to $f \approx 2.5$ kHz are shown in Fig. 3. Both the continuous measurements (continuous lines) of swept B-field values and those at fixed B-field (solid points) clearly indicate a frequency dependence. The black stars represent the CCC data points representing the dc values. When plotting the ρ_{xx} values with respect to the applied frequency f, one finds a mostly linear frequency dependence. The differences between the ac values extrapolated to 0 Hz, and the results of the CCC measurements were found to be below 50 $\mu\Omega$ when taking the type B uncertainties of the two measurements into account. This linear relationship is also known from GaAs devices [30] and follows the term:

$$Z_{xx} = R_{xx} + \omega \cdot R_{xy}^2 \cdot C \cdot [j + \tan\delta]$$

where Z_{xx} is the measured impedance, ω is the angular frequency, C is the parallel capacitance, and $\tan(\delta)$ is the associated dissipation factor. The mostly linear relationship implies that the frequency dependence of both C and $\tan(\delta)$ is very small and may be neglected. The plotted ac longitudinal resistances ρ_{xx} in Fig. 3 describe the real part of Z_{xx}.

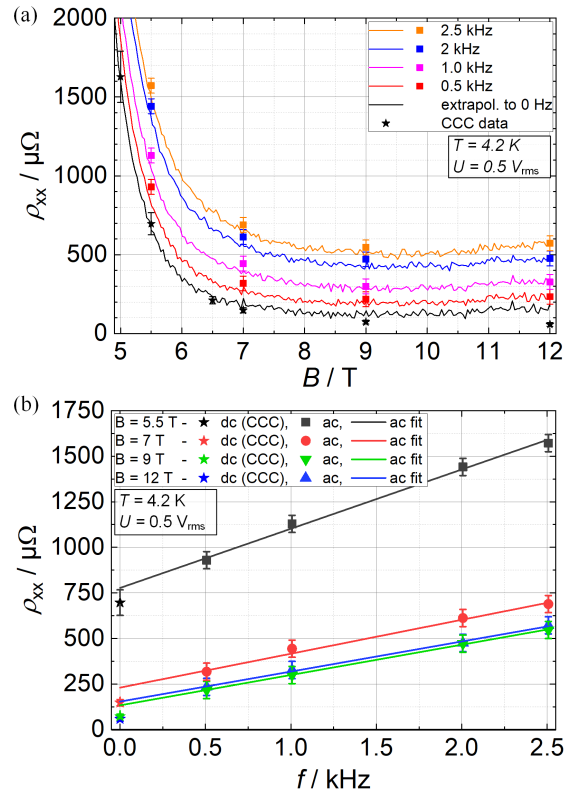

Fig. 3. Longitudinal resistance measurements of device 1 at ac and a comparison to the dc results. (a) and (b) B-field and frequency dependence of ρ_{xx}. The real part of the longitudinal resistance shows a linear frequency dependence. The extrapolated results (least square fit) are in good agreement with dc precision measurements.

A straightforward way to determine the characteristic capacitances and related losses in the device is to use the left side of the attached double shield as an electrode. Fig. 4(a) represents the magnetocapacitance measurement configuration of C_x between the active electrode (left side) and the graphene Hall bar between port A and port B in Fig. 4(a) by comparing C_x with a 1422-CD variable precision reference capacitor in a simple bridge configuration as described in the literature [26]. Since the passive electrode (right side) is shorted to the graphene Hall bar, it does not contribute to the measurement of C_x. The differently colored graphene regions are simplified representations the of compressible and incompressible states in the 2-D electron gas of the Hall bar. In reality, the regions can have different shapes and structures on the nanometer scale due to local variations in the transport properties [31]–[36].

Fig. 4(b) and (c) shows the voltage and frequency dependencies of the magnetocapacitance and the associated dissipation factor for device 1 that can be best explained by the model of compressible and incompressible states. At low B-field values, the 2-D electron gas in the graphene is in a nonquantized state, similar to metal, with mostly compressible states. When increasing the B-field, the capacitance C_x starts dropping around $B = 4$ T and decreases by about 3 fF in both the cases when approaching $B = 12$ T due to the increase in incompressible areas that are transparent to the electrical field. Simultaneously, the dissipation factor first

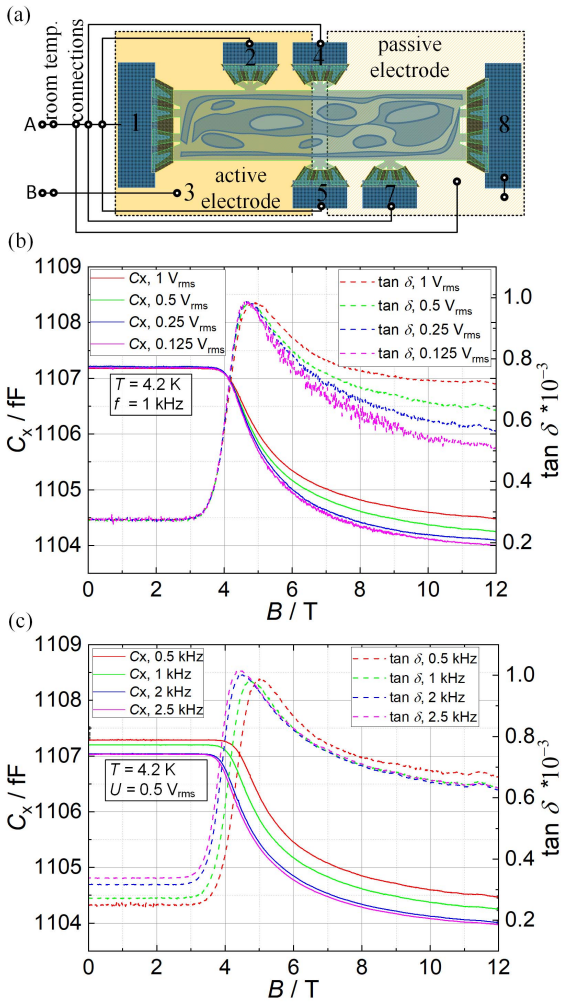

Fig. 4. Magnetocapacitance measurements of device 1 at 4.2 K. (a) Drawing describes magnetocapacitance measurement configuration. While one electrode is shorted to pin 8 (passive electrode), the left electrode (active electrode) is used to characterize C and tan(δ). The graphene areas with regions of different colors and brightness are simplified representations of compressible and incompressible states in the 2-D electron gas of the Hall bar. (b) Voltage dependence. (c) Frequency dependence of the magnetocapacitance C_x and the loss factor tan(δ) between the active electrode and the graphene Hall bar device.

increases and peaks in the transition region when entering the resistance plateau, which describes a significant increase in dissipation. Once the quantization improves at higher B-field, the dissipative losses then again decrease to a level of about $\tan(\delta) = 0.0003$ compared with the value at zero B-field. The magnetocapacitance measurement (Fig. 4) shows the transition of the electronic state not only in the same magnetic field range as a dc precision measurement (Fig. 2) but also in more physical detail. Thus, the measured quantities are well-suited to identify where the device is best quantized. We note that the multimeter measurement shown in Fig. 1(a) indicates the transition to the quantized state at a considerably lower magnetic field, but this is just an artifact due to the coarse scale.

While GaAs-based QHE devices exhibit a voltage dependence but no frequency dependence of C_x and tan(δ) [26],

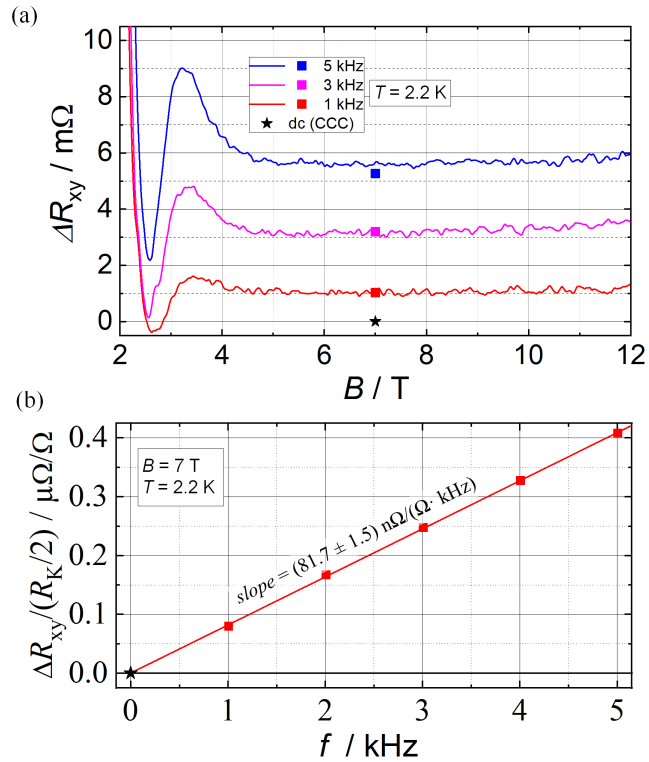

Fig. 5. Hall resistance measurements of device 2 at ac and a comparison to results at direct current (black star). (a) and (b) AC measurements of the Hall resistance show a linear frequency dependence between 0 and 5 kHz. ΔR_{xy} is the difference between the real part of the measured ac Hall resistance and $R_K/2$.

weak but measurable dependencies of both types were identified in the case of the graphene device in this work. Previous measurements of double-shielded graphene QHE devices that applied photochemical doping for charge carrier density control showed dissipation factor and capacitance values on the same order of magnitude and weak dependencies of both types [27]. This indicates that the behavior is common in the case of graphene also when using different doping techniques. Though the influence of the SiC substrate is expected not to contribute [27], it is possible that the applied doping layer, for example, $Cr(CO)_3$ plays a role in the observed weak frequency dependence.

V. AC Precision Measurements

For verification of the suitability of $Cr(CO)_3$ functionalized graphene Hall devices for metrological purposes at ac, a second device was characterized and used for precision impedance measurements. Device 2 was initially characterized in a similar way as device 1 at dc to find a good working point for precision measurements of the Hall resistance. Fig. 5 shows the precision measurements of the real part of the ac Hall resistance R_{xy} at ac, which was characterized using a transformer-based coaxial impedance bridge setup as described in [3]. Fig. 5(a) shows the absolute deviation of R_{xy} from the value of the QHR due to superimposed capacitive dissipation. The measurements at continuously changing magnetic flux densities between $B = 2$ T and $B = 12$ T (solid lines) show

a typical behavior with an oscillation at the beginning of the resistance plateau as well as a broad and mostly flat region for $B \geq 5$ T. The precision measurements of R_{xy} at the fixed magnetic flux density of $B = 7$ T are represented by the solid data points.

Fig. 5(b) shows that the frequency dependence of the Hall resistance follows a linear characteristic with a slope of (81.7 ± 1.5) (nΩ/(Ω·kHz)). The extrapolated dc value of (0.36 nΩ/Ω ± 2.73 nΩ/Ω) ($k = 1$) is in good agreement with the dc value obtained from the CCC measurement of (−3.37 nΩ/Ω ± 3.5 nΩ/Ω) ($k = 1$). From the observation of a linear characteristic and the term of the impedance of the Hall resistance [30]

$$Z_H = R_{xy}\big(1 \pm \omega \cdot R_{xy} \cdot C \cdot [j + \tan\delta]\big).$$

We can conclude that C and $\tan(\delta)$ are mostly independent of the frequency. From this, we can conclude that the weak dependencies that we found in Section IV are not strong enough to lead to a measurable nonlinear dependence in the real part of the ac Hall resistance.

Previously published ac measurement results of graphene QHE devices often showed a negative linear slope in the frequency dependence and were only found to be positive in the case of very large devices [6], [37]. Positive linear slopes are also known from GaAs-based ac QHE devices, which are also typically relatively large (e.g., width = 0.64 mm × length = 2.6 mm) [38], [39]. However, the devices in this work also show a positive linear slope despite smaller dimensions (width = 0.2 mm × length = 0.8 mm). Since dissipative capacitances between individual parts inside the graphene device, such as contacts and Hall bar edges, cause a negative contribution to the frequency dependence of Z_H, the smaller negative contribution due to the fewer number of Hall contacts compared with the standard design is a possible reason for the positive slope found in this work. Another explanation could be the absence of the double shield for this device which leads to unknown dissipative capacitances between the graphene and the surrounding metals that add a component with a positive contribution.

VI. Conclusion

The presented results demonstrate that $Cr(CO)_3$ functionalized graphene Hall devices provide a well-quantized resistance at dc with a relative deviation from $R_K/2$ of zero within the combined uncertainties. Contact resistances were found to be zero within the measurement uncertainty of 10 mΩ at 1 kHz. Both the ac resistance quantization and the longitudinal resistance of the graphene devices show a linear frequency dependence very similar to GaAs-based QHR standards. The dc and extrapolated ac results agree with each other within their combined uncertainties such that the offset at ac can be precisely modeled. In contrast to a previous work on graphene devices, the slope of the frequency dependence of the Hall resistance was positive. Possible explanations are the fewer number of Hall contacts in the device design or higher dissipative capacitances between the graphene and the surrounding metals due to insufficient shielding. This gives rise to the idea of further engineering the device contacts and shielding to achieve devices that ideally exhibit no frequency dependence. To measure the ac dependencies with more physical detail, the superimposed capacitive dissipation was characterized by magnetocapacitance measurements. The identified frequency dependence of the magnetocapacitance and loss factor was small enough to cause no nonlinear behavior in the Hall and longitudinal resistance values up to at least 2.5 kHz. Additionally, the capacitance and dissipation factor measurements were shown to be useful to identify the window in which the device is best quantized. The presented results demonstrate that graphene devices using branched Hall contacts and $Cr(CO)_3$ functionalization for charge carrier density control are well-suited for precision QHE measurements in the dc and ac regime.

Acknowledgment

The authors would like to thank M. G. Griffin-Ferris, D. B. Newell, C.-I. Liu, G. Fitzpatrick, A. L. Levy, E. C. Benck, and the National Institute of Standards and Technology (NIST) Washington Editorial Review Board for assistance with the internal NIST review process. The work of Dinesh K. Patel at NIST was made possible by arrangement with Prof. C.-T. Liang of the National Taiwan University.

†Commercial equipment, instruments, and materials are identified in this paper in order to specify the experimental procedure adequately. Such identification is not intended to imply recommendation or endorsement by the Physikalisch-Technische Bundesanstalt, the National Institute of Standards and Technology or the United States government, nor is it intended to imply that the materials or equipment identified are necessarily the best available for the purpose.

References

[1] E. Gáábel and U. Siegner, *The New International System of Units*. Hoboken, NJ, USA: Wiley, 2019.

[2] A. F. Rigosi and R. E. Elmquist, "The quantum Hall effect in the era of the new Si," *Semicond. Sci. Technol.*, vol. 34, no. 9, Sep. 2019, Art. no. 093004, doi: 10.1088/1361-6641/ab37d3.

[3] J. Schurr, F. Ahlers, and B. P. Kibble, "The AC quantum Hall resistance as an electrical impedance standard and its role in the Si," *Meas. Sci. Technol.*, vol. 23, no. 12, Dec. 2012, Art. no. 124009, doi: 10.1088/0957-0233/23/12/124009.

[4] J. Schurr, V. Bärkel, and B. P. Kibble, "Realizing the farad from two AC quantum Hall resistances," *Metrologia*, vol. 46, no. 6, pp. 619–628, Dec. 2009, doi: 10.1088/0026-1394/46/6/003.

[5] K. V. Klitzing and G. Ebert, "Application of the quantum Hall effect in metrology," *Metrologia*, vol. 21, no. 1, pp. 11–18, Jan. 1985, doi: 10.1088/0026-1394/21/1/004.

[6] C.-C. Kalmbach *et al.*, "Towards a graphene-based quantum impedance standard," *Appl. Phys. Lett.*, vol. 105, no. 7, Aug. 2014, Art. no. 073511, doi: 10.1063/1.4893940.

[7] L. Callegaro *et al.*, "The EMPIR project GIQS: Graphene impedance quantum standard," in *Proc. Conf. Precis. Electromagn. Meas. (CPEM)*, Aug. 2020, pp. 1–2.

[8] J. Schurr, J. Kuäera, K. Pierz, and B. P. Kibble, "The quantum Hall impedance standard," *Metrologia*, vol. 48, no. 1, pp. 47–57, Feb. 2011, doi: 10.1088/0026-1394/48/1/005.

[9] F. Overney, B. Jeanneret, B. Jeckelmann, B. M. Wood, and J. Schurr, "The quantized Hall resistance: Towards a primary standard of impedance," *Metrologia*, vol. 43, no. 5, pp. 409–413, Oct. 2006, doi: 10.1088/0026-1394/43/5/011.

[10] T. J. B. M. Janssen *et al.*, "Graphene, universality of the quantum Hall effect and redefinition of the Si system," *New J. Phys.*, vol. 13, no. 9, Sep. 2011, Art. no. 093026, doi: 10.1088/1367-2630/13/9/093026.

[11] R. Ribeiro-Palau *et al.*, "Quantum Hall resistance standard in graphene devices under relaxed experimental conditions," *Nature Nanotechnol.*, vol. 10, no. 11, pp. 965–971, Nov. 2015, doi: 10.1038/nnano.2015.192.

[12] A. F. Rigosi *et al.*, "Graphene devices for tabletop and high-current quantized Hall resistance standards," *IEEE Trans. Instrum. Meas.*, vol. 68, no. 6, pp. 1870–1878, Jun. 2019, doi: 10.1109/TIM.2018.2882958.

[13] T. J. B. M. Janssen *et al.*, "Operation of graphene quantum Hall resistance standard in a cryogen-free table-top system," *2D Mater.*, vol. 2, no. 3, Aug. 2015, Art. no. 035015, doi: 10.1088/2053-1583/2/3/035015.

[14] M. Kruskopf *et al.*, "Graphene quantum Hall effect devices for AC and DC resistance metrology," in *Proc. Conf. Precis. Electromagn. Meas. (CPEM)*, Aug. 2020, pp. 1–2.

[15] A. F. Rigosi *et al.*, "Electrical stabilization of surface resistivity in epitaxial graphene systems by amorphous boron nitride encapsulation," *ACS Omega*, vol. 2, no. 5, pp. 2326–2332, May 2017, doi: 10.1021/acsomega.7b00341.

[16] M. Kruskopf and R. E. Elmquist, "Epitaxial graphene for quantum resistance metrology," *Metrologia*, vol. 55, no. 4, pp. R27–R36, Aug. 2018, doi: 10.1088/1681-7575/aacd23.

[17] M. Kruskopf *et al.*, "Two-terminal and multi-terminal designs for next-generation quantized Hall resistance standards: Contact material and geometry," *IEEE Trans. Electron Devices*, vol. 66, no. , pp. 3973–3977, Sep. 2019, doi: 10.1109/TED.2019.2926684.

[18] F. Delahaye, "Series and parallel connection of multiterminal quantum Hall-effect devices," *J. Appl. Phys.*, vol. 73, no. 11, pp. 7914–7920, Jun. 1993, doi: 10.1063/1.353944.

[19] F. Delahaye, B. P. Kibble, and A. Zarka, "Controlling AC losses in quantum Hall effect devices," *Metrologia*, vol. 37, no. 6, pp. 659–670, Dec. 2000, doi: 10.1088/0026-1394/37/6/3.

[20] M. E. Cage and A. Jeffery, "A problem in AC quantized Hall resistance measurements and a proposed solution," *J. Res. Nat. Inst. Standards Technol.*, vol. 103, no. 6, p. 593, Nov. 1998, doi: 10.6028/jres.103.038.

[21] A. F. Rigosi *et al.*, "Gateless and reversible Carrier density tunability in epitaxial graphene devices functionalized with chromium tricarbonyl," *Carbon*, vol. 142, pp. 468–474, Feb. 2019, doi: 10.1016/j.carbon.2018.10.085.

[22] M. Yang *et al.*, "Puddle-induced resistance oscillations in the breakdown of the graphene quantum Hall effect," *Phys. Rev. Lett.*, vol. 117, no. 23, Dec. 2016, Art. no. 237702, doi: 10.1103/PhysRevLett.117.237702.

[23] B. Jeanneret, "AC QHR sample holder," EURAMET, Brunswick, Germany, Tech. Rep. Euromet Project 540, 2001.

[24] J. Schurr, B. P. Kibble, G. Hein, and K. Pierz, "Controlling losses with gates and shields to perfect a quantum Hall impedance standard," *IEEE Trans. Instrum. Meas.*, vol. 58, no. 4, pp. 973–979, Apr. 2009, doi: 10.1109/TIM.2008.2006961.

[25] B. P. Kibble and J. Schurr, "A novel double-shielding technique for AC quantum Hall measurement," *Metrologia*, vol. 45, no. 5, pp. L25–L27, Oct. 2008, doi: 10.1088/0026-1394/45/5/N01.

[26] J. Schurr, F. Ahlers, and K. Pierz, "Magnetocapacitance and loss factor of GaAs quantum Hall effect devices," *Metrologia*, vol. 51, no. 3, pp. 235–242, 2014, doi: 10.1088/0026-1394/51/3/235.

[27] J. Schurr *et al.*, "Magnetocapacitance and dissipation factor of epitaxial graphene-based quantum Hall effect devices," *Phys. Rev. B, Condens. Matter*, vol. 96, no. 15, Oct. 2017, Art. no. 155443, doi: 10.1103/PhysRevB.96.155443.

[28] F. Delahaye and B. Jeckelmann, "Revised technical guidelines for reliable DC measurements of the quantized Hall resistance," *Metrologia*, vol. 40, no. 5, pp. 217–223, Oct. 2003, doi: 10.1088/0026-1394/40/5/302.

[29] F. Delahaye, "Technical guidelines for reliable measurements of the quantized Hall resistance," *Metrologia*, vol. 26, no. 1, pp. 63–68, Jan. 1989, doi: 10.1088/0026-1394/26/1/005.

[30] J. Schurr *et al.*, "AC longitudinal and contact resistance measurements of quantum Hall devices," *Metrologia*, vol. 43, no. 1, pp. 163–173, Feb. 2006, doi: 10.1088/0026-1394/43/1/021.

[31] D. B. Chklovskii and P. A. Lee, "Transport properties between quantum Hall plateaus," *Surf. Sci.*, vol. 305, nos. 1–3, pp. 133–138, Mar. 1994, doi: 10.1016/0039-6028(94)90873-7.

[32] K. Lier and R. R. Gerhardts, "Self-consistent calculations of edge channels in laterally confined two-dimensional electron systems," *Phys. Rev. B, Condens. Matter*, vol. 50, no. 11, pp. 7757–7767, Sep. 1994, doi: 10.1103/PhysRevB.50.7757.

[33] K. Arai, K. Oto, S. Takaoka, and K. Murase, "Investigation of incompressible region by magnetocapacitance measurement in quantum Hall plateaux," *Phys. E Low-Dimensional Syst. Nanostruct.*, vol. 9, no. 2, pp. 243–249, 2001, doi: 10.1016/S1386-9477(00)00169-7.

[34] K. Panos, R. R. Gerhardts, J. Weis, and K. V. Klitzing, "Current distribution and Hall potential landscape towards breakdown of the quantum Hall effect: A scanning force microscopy investigation," *New J. Phys.*, vol. 16, no. 11, Nov. 2014, Art. no. 113071, doi: 10.1088/1367-2630/16/11/113071.

[35] R. Woltjer, "Model for the quantised Hall effect due to inhomogeneities," *Semicond. Sci. Technol.*, vol. 4, no. 3, pp. 155–167, Mar. 1989, doi: 10.1088/0268-1242/4/3/005.

[36] E. Guvenilir, O. Kilicoglu, D. Eksi, and A. Siddiki, "Classical and quantum capacitances calculated locally considering a two-dimensional Hall bar," *Phys. E, Low-dimensional Syst. Nanostruct.*, vol. 106, pp. 283–290, Feb. 2019, doi: 10.1016/j.physe.2018.09.010.

[37] F. Luond *et al.*, "AC quantum Hall effect in epitaxial graphene," *IEEE Trans. Instrum. Meas.*, vol. 66, no. 6, pp. 1459–1466, Jun. 2017, doi: 10.1109/TIM.2017.2652501.

[38] J. Schurr, B. M. Wood, and F. Overney, "Linear frequency dependence in AC resistance measurement," *IEEE Trans. Instrum. Meas.*, vol. 54, no. 2, pp. 512–515, Apr. 2005, doi: 10.1109/TIM.2005.843583.

[39] B. Jeanneret and F. Overney, "Phenomenological model for frequency-related dissipation in the quantized Hall resistance," *IEEE Trans. Instrum. Meas.*, vol. 56, no. 2, pp. 431–434, Apr. 2007, doi: 10.1109/TIM.2007.891162.